

Slow Motion of a General Axisymmetric Slip Particle Along Its Axis of Revolution and Normal to One or Two Plane Walls

Huan J. Keh¹ and Yu C. Chang²

Abstract: A theoretical study of the Stokes flow caused by a rigid particle of revolution translating axisymmetrically perpendicular to two parallel plane walls at an arbitrary position between them in a viscous fluid, which may slip at the particle surface, is presented. A method of distribution of a set of spherical singularities along the axis of revolution within a prolate particle or on the fundamental plane within an oblate particle is used to find the general solution of the fluid velocity field that satisfies the boundary conditions at the plane walls and at infinity. The slip condition on the particle surface is then satisfied by applying a boundary collocation technique to this general solution to determine the unknown constants. The drag force acting on the particle by the fluid is calculated with good convergence behavior for various cases. For the motion of a slip sphere perpendicular to two plane walls, our drag results agree very well with the numerical solutions previously obtained. For the translation of a no-slip prolate or oblate spheroid along its axis of revolution normal to a single plane wall, the agreement between our results and the available solutions in the literature is also excellent. It is found that for a spheroid with specified aspect ratio and particle-to-wall spacings, its boundary-corrected drag force in general decreases with an increase in its slip coefficient. For given wall-to-wall spacings, the hydrodynamic drag force is minimal when the particle is situated midway between the two plane walls and increases monotonically when it approaches either of the walls. For fixed separation and slip parameters, the normalized drag force increases with a decrease in its axial-to-radial aspect ratio, and the boundary effect on the motion of an oblate spheroid can be very significant.

Keywords: Creeping flow, Axisymmetric particle, Prolate and oblate spheroids, Slip-flow surface, Boundary effect, Hydrodynamic drag force, Singularity method,

¹ Corresponding Author: Department of Chemical Engineering, National Taiwan University, Taipei, 10617, Taiwan, Republic of China. E-mail: huan@ntu.edu.tw

² Department of Chemical Engineering, National Taiwan University, Taipei, 10617, Taiwan, Republic of China

Boundary collocation technique

1 Introduction

The movement of small particles in a viscous fluid at low Reynolds numbers is of much fundamental and practical interest in the fields of chemical, biomedical, and environmental engineering and colloidal science. The majority of these moving phenomena is fundamental in nature, but permits one to develop rational understanding of many practical systems and industrial processes such as sedimentation, coagulation, meteorology, motion of cells in blood vessels, and rheology of suspensions. The theoretical treatment of this subject grew out of the classic work of Stokes (1851) for a translating, no-slip, rigid sphere in an incompressible, Newtonian fluid. Oberbeck (1876) extended this result to the translation of an ellipsoid. More recently, the creeping flow caused by the motion of a particle of more general shape has been treated in the literature by the symbolic operator method [Brenner (1966)], boundary collocation method [O'Brien (1968); Gluckman, Pfeffer, and Weinbaum (1971)], singularity method [Chwang and Wu (1975)], and boundary integral/element method [Hsu and Ganatos (1989); Staben, Zinchenko, and Davis (2003); Sellier (2008)].

In the general formulation of the Stokes problem, it is usually assumed that no slippage arises at the solid-fluid interfaces. Actually, this is an idealization of the transport processes involved. The phenomena that the adjacent fluid can slip frictionally over a solid surface, occurring for cases such as the rarefied gas flow surrounding an aerosol particle [Ying and Peters (1991); Hutchins, Harper, and Felder (1995)], the aqueous liquid flow near a hydrophobic surface [Tretheway and Meinhart (2002); Willmott (2008)], the micropolar fluid flow past a rigid particle [Sherif, Faltas, and Saad (2008)], and the Newtonian fluid flow over the surface of a porous medium [Saffman (1971); Nir (1976)] or a small particle of molecular size [Hu and Zwanzig (1974)], have been confirmed, both experimentally and theoretically. Presumably, any such slipping would be proportional to the local tangential stress of the fluid next to the solid surface [Happel and Brenner (1983)], known as the Navier slip [see Eq. (3a)], at least as long as the velocity gradient is small. The constant of proportionality, β^{-1} , is called the slip coefficient of the solid surface.

The classic formula for the drag force exerted by the ambient fluid of viscosity η on a translating rigid sphere of radius b with a slip-flow boundary condition at its surface, first derived by Basset (1961), is

$$F = -6\pi\eta bU \frac{\beta b + 2\eta}{\beta b + 3\eta}, \quad (1)$$

where U is the translational velocity of the particle. The quantity η/β is a length,

which can be pictured by noting that the fluid motion is the same as if the solid surface was displaced inward by a distance η/β with the velocity gradient extending uniformly right up to no-slip velocity at the surface. In the limiting case of $\eta/\beta b = 0$, there is no slip at the particle surface and Eq. (1) degenerates to the well-known Stokes law. When $\eta/\beta b \rightarrow \infty$, there is a perfect slip at the particle surface and the particle acts like a spherical gas bubble (with negligible viscosity).

The problem of slow motion of nonspherical particles with frictionally slip surfaces is a matter of great analytical difficulty and was usually estimated by an adjusted sphere approximation [Dahneke (1973)]. On the other hand, the axisymmetric creeping flow of a viscous incompressible fluid past a spheroid which deforms slightly in shape from a sphere with the slip boundary condition was investigated by several researchers [Palaniappan (1994); Ramkissoon (1997)], and an explicit expression for the hydrodynamic drag force experienced by it was given to the first order in the small parameter characterizing the deformation. Recently, the motion of a slightly deformed slip sphere in an arbitrary direction was also analyzed to the second order of the small deformation parameter [Chang and Keh (2009)].

Knowing that a simple separation-of-variable solution for the problem of the slow motion of a spheroid with a frictional-slip surface in a viscous fluid is not feasible in prolate and oblate spheroidal coordinates [Leong (1984); Williams (1986)], Keh and Huang (2004) investigated the creeping flow caused by a general axisymmetric particle with a slip surface translating along its axis of revolution numerically by using a method of internal singularity distributions incorporated with a boundary collocation technique. In fact, a semi-separable general solution in the form of an infinite series expansion for the axisymmetric creeping flow in spheroidal coordinates was used by Deo and Datta (2002) to examine the slip flow of a viscous fluid axisymmetrically past a prolate spheroid and to derive the hydrodynamic drag force exerted on the spheroid in an approximate but explicit form. Recently, we studied the axisymmetric translation of a prolate or oblate slip spheroid and obtained the drag force both analytically by employing the same semi-separable solution and numerically by using the boundary collocation method (Keh and Chang, 2008).

In practical applications of colloidal transport, particles are not isolated and will move in the presence of neighboring boundaries. Therefore, the boundary effects on creeping motion of rigid particles experiencing slip are of great importance and have been studied in the past for several cases of a confined sphere [Chen and Keh (2003); Chang and Keh (2006); Keh and Chang (2007)]. Recently, the transverse motion of a slip circular cylinder near a plane wall parallel to its axis has also been investigated semianalytically [Keh and Wang (2008)]. In this article we use a method of distributed internal singularities incorporated with the boundary collocation technique [Wan and Keh (2010)] to analyze the creeping motion a slip particle

of revolution translating axisymmetrically perpendicular to two plane walls at an arbitrary position between them; the particle can be either prolate or oblate. With this approach the drag force exerted on a spheroid by the ambient fluid as functions of the slip coefficient, the separation distances from the walls, the relative position between the walls, and the aspect ratio of the spheroid is numerically calculated. For the special cases of a slip sphere and a no-slip spheroid, our drag results show excellent agreement with those available in the literature.

2 Mathematical description of the general problem

In this section, we consider the quasisteady creeping motion caused by a general axisymmetric particle translating with a constant velocity $U\mathbf{e}_z$ in an incompressible, Newtonian fluid along its axis of revolution and perpendicular to two infinite parallel plane walls whose distances from the center of the particle are c and d , respectively ($d \geq c$ is set without loss in generality), as shown in Fig. 1. Here (ρ, ϕ, z) and (r, θ, ϕ) denote the circular cylindrical and spherical coordinate systems, respectively, with their origin lying at the center of the particle, and \mathbf{e}_z is the unit vector in the positive z direction. The fluid may slip frictionally at the surface of the particle and is at rest at infinity. The Reynolds number is assumed to be sufficiently small so that the inertial terms in the fluid momentum equation can be neglected, in comparison with the viscous terms.

The fluid flow is governed by the Stokes equations,

$$\eta \nabla^2 \mathbf{v} - \nabla p = \mathbf{0}, \quad (2a)$$

$$\nabla \cdot \mathbf{v} = 0, \quad (2b)$$

where \mathbf{v} is the velocity field for the fluid flow and p is the dynamic pressure distribution. Because the relative tangential velocity of the fluid at the particle surface is proportional to the local tangential stress and the fluid is no-slip on the plane walls and motionless far away from the particle, the boundary conditions are

$$\mathbf{v} = U\mathbf{e}_z + \frac{1}{\beta}(\mathbf{I} - \mathbf{n}\mathbf{n})\mathbf{n} : \boldsymbol{\tau} \text{ on } S_p, \quad (3a)$$

$$\mathbf{v} = \mathbf{0} \text{ at } z = -c, d, \quad (3b)$$

$$\mathbf{v} \rightarrow \mathbf{0} \text{ as } \rho \rightarrow \infty \text{ and } -c \leq z \leq d. \quad (3c)$$

Here, $\boldsymbol{\tau} = \eta[\nabla \mathbf{v} + (\nabla \mathbf{v})^T]$ is the viscous stress tensor for the fluid which is symmetric, \mathbf{n} is the unit normal vector on the particle surface S_p pointing into the fluid, \mathbf{I} is the unit dyadic, and $1/\beta$ is the constant frictional-slip coefficient about the surface of the particle.

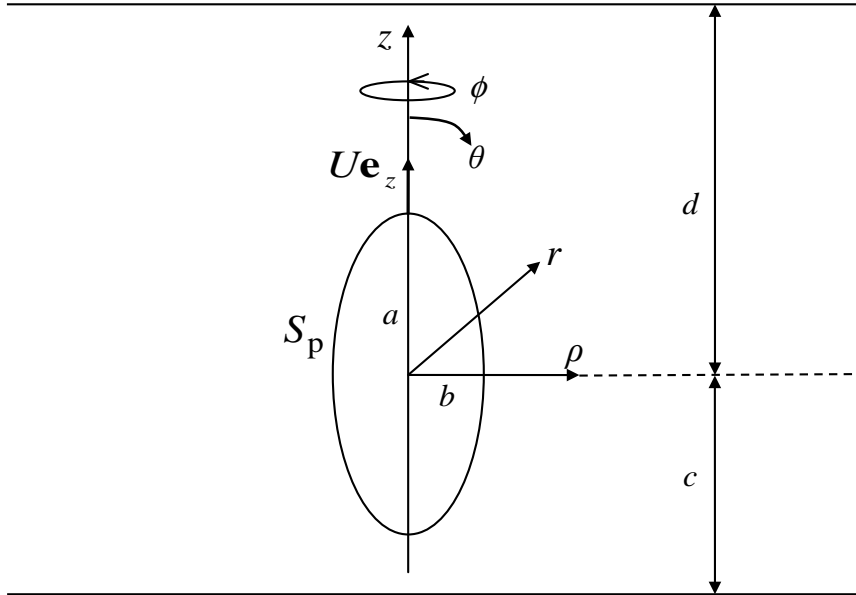


Figure 1: Geometrical sketch for the translation of an axially symmetric particle along its axis of revolution perpendicular to two plane walls.

In order to solve Eqs. (2) and (3), a set of spherical singularities satisfying the boundary conditions in Eqs. (3b) and (3c) will be chosen and distributed along the axis of revolution within a prolate particle or on the fundamental plane within an oblate particle [Keh and Tseng (1994)]. The flow field surrounding the particle is approximated by the superposition of the set of the spherical singularities and the boundary condition (3a) on the particle surface can be satisfied by making use of the multipole collocation method. For the special case of a spherical particle, only a single singularity which is placed at the particle center is needed.

The velocity components in circular cylindrical coordinates for the axially symmetric fluid motion caused by a spherical singularity at the point \$\rho = 0\$ and \$z = h\$ satisfying the Stokes equations and boundary conditions in Eqs. (3b) and (3c) are [Ganatos, Weinbaum, and Pfeffer (1980); Chang and Keh (2006)]

$$v_\rho = \sum_{n=2}^{\infty} [B_n A_{1n}(\rho, z, h) + D_n A_{2n}(\rho, z, h)], \quad (4a)$$

$$v_z = \sum_{n=2}^{\infty} [B_n C_{1n}(\rho, z, h) + D_n C_{2n}(\rho, z, h)], \quad (4b)$$

and $v_\phi = 0$. Here, A_{in} and C_{in} with $i = 1$ and 2 are functions defined by Eqs. (A1) and (A2) in Appendix A, and B_n and D_n are unknown constants.

In cylindrical coordinates, the boundary condition (3a) on the particle surface can be expressed as

$$\left. \begin{aligned} v_\rho &= \frac{1}{\beta} [(1 - n_\rho^2)n_\rho \tau_{\rho\rho} - n_\rho n_z^2 \tau_{zz} + (1 - 2n_\rho^2)n_z \tau_{\rho z}] \\ v_z &= U + \frac{1}{\beta} [(1 - n_z^2)n_z \tau_{zz} - n_z n_\rho^2 \tau_{\rho\rho} + (1 - 2n_z^2)n_\rho \tau_{\rho z}] \end{aligned} \right\} \text{on } S_p \quad (5)$$

where n_ρ and n_z are the local ρ and z components of the unit normal vector \mathbf{n} . From Eq. (4) the components of the viscous stress tensor in Eq. (5) caused by the singularity are obtained as

$$\tau_{\rho\rho} = \eta \sum_{n=2}^{\infty} [B_n \alpha_{1n}(\rho, z, h) + D_n \alpha_{2n}(\rho, z, h)], \quad (6a)$$

$$\tau_{zz} = \eta \sum_{n=2}^{\infty} [B_n \beta_{1n}(\rho, z, h) + D_n \beta_{2n}(\rho, z, h)], \quad (6b)$$

$$\tau_{\rho z} = \eta \sum_{n=2}^{\infty} [B_n \gamma_{1n}(\rho, z, h) + D_n \gamma_{2n}(\rho, z, h)], \quad (6c)$$

where α_{in} , β_{in} , and γ_{in} with $i = 1$ and 2 are functions defined by Eqs. (A3)-(A5).

Eqs. (4) and (6) for the fluid velocity and stress fields caused by a spherical singularity and boundary condition (5) on the particle surface will be utilized in the following sections to solve for the fluid velocity induced by the translation of an axially symmetric particle along its axis of revolution normal to two plane walls.

3 Solution for the motion of a spherical particle normal to two plane walls

A spherical singularity described in the previous section is used in this section to obtain the solution for the motion of a slip spherical particle of radius b perpendicular to two plane walls. The flow field generated by the translation of the sphere can be represented by a singularity placed at its center which is the origin of the coordinate frame. Thus, the velocity and stress components for the fluid motion caused by the sphere are given by Eqs. (4) and (6) with $h = 0$. To determine the unknown constants B_n and D_n , one can apply the boundary condition (5) at the particle surface to these velocity and stress components to yield

$$\left. \begin{aligned} \sum_{n=2}^{\infty} [B_n A_{1n}^*(\rho, z, 0) + D_n A_{2n}^*(\rho, z, 0)] &= 0 \\ \sum_{n=2}^{\infty} [B_n C_{1n}^*(\rho, z, 0) + D_n C_{2n}^*(\rho, z, 0)] &= U \end{aligned} \right\} \text{at } r = b, \quad (7)$$

where

$$\begin{aligned} A_{in}^*(\rho, z, h) &= A_{in}(\rho, z, h) - \frac{\eta}{\beta} [(1 - n_\rho^2)n_\rho \alpha_{in}(\rho, z, h) - n_\rho n_z^2 \beta_{in}(\rho, z, h) \\ &\quad + (1 - 2n_\rho^2)n_z \gamma_{in}(\rho, z, h)], \end{aligned} \quad (8a)$$

$$\begin{aligned} C_{in}^*(\rho, z, h) &= C_{in}(\rho, z, h) - \frac{\eta}{\beta} [(1 - n_z^2)n_z \beta_{in}(\rho, z, h) - n_z n_\rho^2 \alpha_{in}(\rho, z, h) \\ &\quad + (1 - 2n_z^2)n_\rho \gamma_{in}(\rho, z, h)], \end{aligned} \quad (8b)$$

and $i = 1$ or 2 .

The drag force $\mathbf{F} = F \mathbf{e}_z$ exerted by the fluid on the spherical particle can be determined from [Ganatos, Weinbaum, and Pfeffer (1980)]

$$F = 4\pi\eta D_2. \quad (9)$$

That is, only the lowest-order coefficient D_2 of the spherical singularity contributes to the hydrodynamic drag on the particle.

To satisfy Eq. (7) exactly along the entire half-circular generating arc of the particle in a meridian plane (from $\theta = 0$ to $\theta = \pi$) would require the solution of the entire infinite array of unknown constants B_n and D_n . However, the multipole collocation method [Ganatos, Weinbaum, and Pfeffer (1980); Keh and Tseng (1994)] enforces the boundary condition at a finite number of discrete points on the generating arc of the sphere and truncates the infinite series in Eqs. (4), (6), and (7) into finite ones. If the spherical boundary is approximated by satisfying the condition of Eq. (7) at N discrete points on its generating arc, then the infinite series are truncated after N terms, resulting in a system of $2N$ simultaneous linear algebraic equations in the truncated form of Eq. (7). This matrix equation can be solved by any matrix-reduction technique to yield the $2N$ unknown constants B_n and D_n required in the truncated form of Eq. (4) for the fluid velocity field. The hydrodynamic drag force acting on the particle can be obtained from Eq. (9) once these coefficients are solved for a sufficiently large value of N . The accuracy of the boundary-collocation/truncation technique can be improved to any degree by taking a sufficiently large value of N . In principle, the truncation error vanishes as $N \rightarrow \infty$.

When selecting the points along the half-circular generating arc of the sphere where the boundary condition (7) is exactly satisfied, the first point that should be chosen is $\theta = \pi/2$, since this point defines the projected area of the particle normal to the direction of motion. In addition, the points $\theta = 0$ and $\theta = \pi$, which control the gaps between the particle and the plane walls, are also important. However,

an examination of the system of linear algebraic Eq. (7) shows that the coefficient matrix becomes singular if these points are used. To overcome the difficulty of singularity and to preserve the geometric symmetry of the particle surface about the equatorial plane $\theta = \pi/2$, points at $\theta = \alpha, \pi/2 - \alpha, \pi/2 + \alpha$, and $\pi - \alpha$ are taken to be four basic collocation points. Additional points along the boundary are selected as mirror-image pairs about the plane $\theta = \pi/2$ to divide the θ coordinate into equal parts. The range of optimum values of α has been found to be quite broad, and here we use 0.01° , with which the numerical results of the hydrodynamic drag force exerted on the particle can converge to at least five significant figures. In principle, as long as the number of the collocation points is sufficiently large and the distribution of the collocation points is adequate, the solution of the drag force will converge and the shape of the particle can be well approximated.

A number of numerical solutions of the dimensionless drag force $-F/6\pi\eta bU$ for the motion of a sphere normal to two plane walls are presented in Table 1 for various values of the parameters b/c , $c/(c+d)$, and $\eta/\beta b$ using the boundary collocation technique [where $c/(c+d) = 0$ represents the case of a single plane wall]. All of the results were obtained by increasing the number of collocation points N until the convergence of at least five significant digits is achieved. To achieve this convergence, the larger value of N is required as the particle is situated closer to the plane walls. The numerical solutions for $-F/6\pi\eta bU$ obtained previously [Chang and Keh (2006)] are also listed (in parentheses) in Table 1 for comparison. It can be seen that the present results from the collocation method agree excellently with the previous results for the desired accuracy and the rate of convergence is quite rapid.

4 Axisymmetric motion of a prolate particle normal to two plane walls

In this section, we consider the translational motion of a general prolate axisymmetric particle along its axis of revolution perpendicular to two plane walls. A segment between points A($\rho = 0, z = -c_1$) and B($\rho = 0, z = c_2$) is taken along the axis of revolution within the particle on which a set of spherical singularities are distributed (c_1 and c_2 are positive constants). If the nose and tail of the particle are round, then their centers of curvature can be chosen as A and B. The general solution of the fluid velocity can be constructed by the superposition of the spherical singularities distributed on the segment AB, and Eq. (4) is used to result in the integral form

$$\begin{bmatrix} v_\rho \\ v_z \end{bmatrix} = \sum_{n=2}^{\infty} \int_{-c_1}^{c_2} \{ B_n(t) \begin{bmatrix} A_{1n}(\rho, z, t) \\ C_{1n}(\rho, z, t) \end{bmatrix} + D_n(t) \begin{bmatrix} A_{2n}(\rho, z, t) \\ C_{2n}(\rho, z, t) \end{bmatrix} \} dt. \quad (10)$$

The corresponding integral expressions for the components of the viscous stress tensor can be obtained accordingly using Eq. (6). Equation (10) provides an exact

solution to Eq. (2) that satisfies Eqs. (3b) and (3c), and the unknown density distribution functions for the singularities, $B_n(t)$ and $D_n(t)$, must be determined from the remaining boundary condition (5) using the multipole collocation technique. From Eqs. (9) and (10), the drag force acting on the prolate particle by the fluid can be expressed as

$$F = 4\pi\eta \int_{-c_1}^{c_2} D_2(t) dt. \quad (11)$$

In order to use the multipole collocation technique to satisfy the boundary condition at the particle surface, the integration encountered in Eqs. (10) and (11) must be treated numerically. Here, we use the M -point Gauss-Legendre quadrature formula [Hornbeck (1975)]

$$\int_{-c_1}^{c_2} f(q) dq = \frac{1}{2}(c_1 + c_2) \sum_{m=1}^M w_m f(q_m), \quad (12)$$

where $f(q)$ is any function of q , q_m are the quadrature zeros, and w_m are the corresponding quadrature weights.

Applying Eq. (12) to Eq. (10) and truncating the infinite series after N terms, we obtain

$$\begin{bmatrix} v_p \\ v_z \end{bmatrix} = \sum_{n=2}^{N+1} \sum_{m=1}^M \left\{ B_{nm} \begin{bmatrix} A_{1n}(\rho, z, q_m) \\ C_{1n}(\rho, z, q_m) \end{bmatrix} + D_{nm} \begin{bmatrix} A_{2n}(\rho, z, q_m) \\ C_{2n}(\rho, z, q_m) \end{bmatrix} \right\}, \quad (13)$$

where B_{nm} and D_{nm} are the unknown density constants. Accordingly, the corresponding stress components are expressed using Eq. (6) as

$$\begin{bmatrix} \tau_{\rho\rho} \\ \tau_{zz} \\ \tau_{\rho z} \end{bmatrix} = \eta \sum_{n=2}^{N+1} \sum_{m=1}^M \left\{ B_{nm} \begin{bmatrix} \alpha_{1n}(\rho, z, q_m) \\ \beta_{1n}(\rho, z, q_m) \\ \gamma_{1n}(\rho, z, q_m) \end{bmatrix} + D_{nm} \begin{bmatrix} \alpha_{2n}(\rho, z, q_m) \\ \beta_{2n}(\rho, z, q_m) \\ \gamma_{2n}(\rho, z, q_m) \end{bmatrix} \right\}. \quad (14)$$

Application of the boundary condition (5) to Eqs. (13) and (14) yields

$$\sum_{n=2}^{N+1} \sum_{m=1}^M \left\{ B_{nm} \begin{bmatrix} A_{1n}^*(\rho, z, q_m) \\ C_{1n}^*(\rho, z, q_m) \end{bmatrix} + D_{nm} \begin{bmatrix} A_{2n}^*(\rho, z, q_m) \\ C_{2n}^*(\rho, z, q_m) \end{bmatrix} \right\} = \begin{bmatrix} 0 \\ U \end{bmatrix} \text{ on } S_p, \quad (15)$$

where the functions A_{in}^* and C_{in}^* with $i = 1$ and 2 are given by Eq. (8). The multipole collocation method allows the boundary of the particle to be approximated by satisfying Eq. (15) at MN discrete values of z or θ (with a constant ϕ) on its surface and results in a set of $2MN$ simultaneous linear algebraic equations, which can be

Table 1: The dimensionless drag force experienced by a spherical particle normal to a single plane wall [$c/(c+d) = 0$] and to two parallel plane walls [$c/(c+d) = 1/4$ and $1/2$]

$\frac{c}{c+d}$	$\frac{\eta}{\beta b}$	$-F/6\pi\eta bU$							
		N	$b/c = 0.1$	N	$b/c = 0.5$	N	$b/c = 0.9$	N	$b/c = 0.99$
0	0	6	1.12619	10	2.12554	28	10.44054	102	100.8942
		10	1.12619	14	2.12554	32	10.44054	106	100.8942
			(1.12619)		(2.12554)		(10.44054)		(100.8942)
0	1	4	0.81902	8	1.28939	22	4.05024	94	27.78722
		8	0.81902	12	1.28939	26	4.05024	98	27.78722
			(0.81902)		(1.28939)		(4.05024)		(27.78722)
0	∞	4	0.72073	10	1.08255	28	3.42001	94	26.38005
		8	0.72073	14	1.08255	32	3.42001	98	26.38005
			(0.72073)		(1.08255)		(3.42001)		(26.38003)
1/4	0	4	1.12812	8	2.15071	28	10.54051	98	101.0228
		8	1.12812	12	2.15071	32	10.54051	102	101.0228
			(1.12811)		(2.15071)		(10.54051)		(101.0227)
1/4	1	4	0.82004	8	1.29996	26	4.08700	98	27.83362
		8	0.82004	12	1.29996	30	4.08700	102	27.83362
			(0.82004)		(1.29997)		(4.08700)		(27.83362)
1/4	∞	4	0.72152	8	1.09012	24	3.44539	94	26.41202
		8	0.72152	12	1.09012	28	3.44539	98	26.41202
			(0.72151)		(1.09012)		(3.44539)		(26.41199)
1/2	0	4	1.16873	10	2.78920	30	19.00391	104	199.8130
		8	1.16873	14	2.78920	34	19.00391	106	199.8130
			(1.16873)		(2.78920)		(19.00351)		(199.8128)
1/2	1	4	0.84144	10	1.56927	26	6.83825	96	54.24891
		8	0.84144	14	1.56927	30	6.83825	100	54.24891
			(0.84144)		(1.56927)		(6.83825)		(54.24892)
1/2	∞	4	0.73809	8	1.29258	28	5.75970	98	51.62672
		8	0.73809	12	1.29258	32	5.75970	102	51.62672
			(0.73809)		(1.29258)		(5.75970)		(51.62687)

*The numerical results in parentheses are obtained from Keh and Chang (2006)

Table 2: The dimensionless drag force experienced by a prolate spheroid translating along its axis of revolution normal to a single plane wall for various values of a/b , a/c , and $\eta/\beta b$

a/b	$\frac{\eta}{\beta b}$	M	$-F/6\pi\eta bU$							
			N	$a/c = 0.1$	N	$a/c = 0.5$	N	$a/c = 0.9$	N	$a/c = 0.99$
1.1	0	4	2	1.13853	2	2.03710	12	8.81357	64	77.7746
			3	1.13852	3	2.03720	13	8.81358	65	77.7755
			4	1.13852	4	2.03720	14	8.81358	66	77.7755
1.1	1	4	2	0.81463	2	1.22706	9	3.48254	66	21.6553
			3	0.81463	3	1.22709	10	3.48252	67	21.6554
			4	0.81463	4	1.22709	11	3.48252	68	21.6554
1.1	∞	4	2	0.70063	3	1.00459	9	2.87280	68	20.3831
			3	0.70064	4	1.00464	10	2.87279	69	20.3830
			4	0.70064	5	1.00464	11	2.87279	70	20.3830
2	0	16	2	1.29139	2	1.83348	2	4.17750	16	17.8005
			3	1.29139	3	1.83348	3	4.17750	17	17.8006
			4	1.29139	4	1.83348	4	4.17750	18	17.8006
2	1	16	2	0.85317	2	1.07064	2	1.82714	17	5.49361
			3	0.85317	3	1.07064	3	1.82714	18	5.49363
			4	0.85317	4	1.07064	4	1.82714	19	5.49363
2	∞	16	2	0.58199	2	0.68459	2	1.16887	15	4.55074
			3	0.58199	3	0.68459	3	1.16887	16	4.55073
			4	0.58199	4	0.68459	4	1.16887	17	4.55073
5	0	20	2	1.85956	2	2.25254	2	3.23465	3	5.17486
			3	1.85956	3	2.25254	3	3.23465	4	5.17500
			4	1.85956	4	2.25254	4	3.23465	5	5.17500
5	1	20	2	1.20696	2	1.36204	2	1.67144	2	2.16078
			3	1.20699	3	1.36208	3	1.67152	3	2.16079
			4	1.20699	4	1.36208	4	1.67152	4	2.16079
5	∞	20	2	0.40639	2	0.42446	2	0.49084	2	0.83239
			3	0.40640	3	0.42447	3	0.49090	3	0.83241
			4	0.40640	4	0.42447	4	0.49090	4	0.83241

solved numerically to yield the $2MN$ density constants B_{nm} and D_{nm} required in Eq. (13) for the fluid velocity field. Once these constants are determined, the drag force exerted by the fluid on the particle can be obtained from Eq. (11), with the result

$$F = 4\pi\eta \sum_{m=1}^M D_{2m}. \quad (16)$$

5 Solution for the axisymmetric motion of a prolate spheroid normal to two plane walls

The method presented in the previous section is used in this section to obtain the solution for the translation of a slip prolate spheroid along its axis of revolution perpendicular to one or two plane walls, as illustrated in Fig. 1. The surface of a spheroid and the local components of its unit normal vector \mathbf{n} in cylindrical coordinates are represented by

$$z(\rho) = \pm a[1 - (\frac{\rho}{b})^2]^{1/2} \quad (17)$$

and

$$n_\rho = \frac{(a/b)^2 \rho}{\sqrt{(a/b)^4 \rho^2 + z^2}}, \quad n_z = \frac{z}{\sqrt{(a/b)^4 \rho^2 + z^2}}, \quad (18)$$

where $0 \leq \rho \leq b$. Depending on the aspect ratio of the spheroid, its shape can range widely from a needle (with $a/b \rightarrow \infty$), to a sphere (with $a/b = 1$), and to a circular disk (with $a/b \rightarrow 0$). For the case of a prolate spheroid, a and b are the major and minor semi-axes, respectively ($1 < a/b < \infty$).

In Section 3, the boundary collocation solutions for the translation of a spherical particle with a slip surface perpendicular to one or two plane walls were presented. We now use the same collocation scheme incorporated with the method of distribution of spherical singularities to obtain the corresponding solution for the axisymmetric motion of a slip prolate spheroid. In Tables 2, the numerical results of the nondimensional hydrodynamic drag force $-F/6\pi\eta bU$ for the translational motion of a prolate spheroid along its axis of revolution perpendicular to a single plane wall [with $c/(c+d) = 0$] are presented for various values of the aspect ratio a/b , spacing parameter a/c , and slip parameter $\eta/\beta b$. The values of $-F/6\pi\eta bU$ are computed for different values of N and M in Eqs. (13)-(16) (which shows convergence tests). To achieve good convergence behavior for the calculation of F , the larger value of N is required when the particle is located closer to the plane wall, whereas the larger value of M is needed when the aspect ratio of the spheroid becomes larger.

In general, the convergence behavior of this method is quite good, except for the extreme case that the particle is very close to the boundary ($a/c > 0.99$). For the special case of a no-slip spheroid (with $\eta/\beta b = 0$), our results agree very well with the previous numerical solutions obtained by Hsu and Ganatos (1989) and Keh and Tseng (1994).

Table 3: The dimensionless drag force experienced by a prolate spheroid situated midway between two parallel plane walls [$c/(c+d) = 1/2$] undergoing axisymmetric translation normal to the walls for various values of a/b , a/c , and $\eta/\beta b$

a/b	$\frac{\eta}{\beta b}$	M	$-F/6\pi\eta bU$							
			N	$a/c = 0.1$	N	$a/c = 0.5$	N	$a/c = 0.9$	N	$a/c = 0.99$
1.1	0	4	2	1.17803	2	2.61926	11	15.7824	59	153.64
			3	1.17802	3	2.61928	12	15.7828	60	153.61
			4	1.17802	4	2.61928	13	15.7828	61	153.61
1.1	1	4	2	0.83478	2	1.46665	11	5.75038	67	42.041
			3	0.83478	3	1.46666	12	5.75037	68	42.040
			4	0.83478	4	1.46666	13	5.75037	69	42.040
1.1	∞	4	2	0.71554	2	1.17686	10	4.73385	66	39.7098
			3	0.71555	3	1.17689	11	4.73386	67	39.7089
			4	0.71555	4	1.17689	12	4.73386	68	39.7089
2	0	10	2	1.31922	2	2.13920	2	6.54384	18	33.7256
			3	1.31922	3	2.13920	3	6.54401	19	33.7258
			4	1.31922	4	2.13920	4	6.54401	20	33.7258
2	1	10	2	0.86527	2	1.18167	2	2.56228	19	9.8641
			3	0.86527	3	1.18167	3	2.56232	20	9.8642
			4	0.86527	4	1.18167	4	2.56232	21	9.8642
2	∞	16	2	0.58762	2	0.73592	2	1.63657	15	8.38350
			3	0.58762	3	0.73593	3	1.63661	16	8.38359
			4	0.58762	4	0.73593	4	1.63661	17	8.38359
5	0	20	2	1.88255	2	2.44590	2	4.17651	3	8.00550
			3	1.88250	3	2.44581	3	4.17633	4	8.00575
			4	1.88250	4	2.44581	4	4.17633	5	8.00575
5	1	20	3	1.21663	3	1.43266	4	1.95279	3	2.90944
			4	1.21662	4	1.43265	5	1.95280	4	2.90947
			5	1.21662	5	1.43265	6	1.95280	5	2.90947
5	∞	20	3	0.40752	3	0.43271	3	0.55322	3	1.23327
			4	0.40749	4	0.43269	4	0.55318	4	1.23330
			5	0.40749	5	0.43269	5	0.55318	5	1.23330

Table 4: The dimensionless drag force experienced by an oblate spheroid translating along its axis of revolution normal to a single plane wall for various values of a/b , a/c , and $\eta/\beta b$

a/b	$\frac{\eta}{\beta b}$	M	$-F/6\pi\eta bU$							
			N	$a/c = 0.1$	N	$a/c = 0.5$	N	$a/c = 0.9$	N	$a/c = 0.99$
0.8	0	4	5	1.11717	5	2.55131	7	16.2982	64	188.40
			6	1.10941	6	2.42886	8	16.2983	65	188.43
			7	1.10941	7	2.42886	9	16.2983	66	188.43
0.8	1	4	5	0.83983	5	1.48707	8	6.03731	68	50.83
			6	0.83933	6	1.49614	9	6.03732	69	50.80
			7	0.83933	7	1.49614	10	6.03732	70	50.80
0.8	∞	4	5	0.77065	5	1.21710	4	5.31456	65	48.924
			6	0.77032	6	1.31601	5	5.31440	66	48.922
			7	0.77032	7	1.31601	6	5.31440	67	48.922
0.5	0	10	4	1.31121	4	3.85184	5	49.7826	30	734.12
			5	1.13142	5	3.85167	6	49.7747	31	734.13
			6	1.13142	6	3.85167	7	49.7747	32	734.13
0.5	1	10	5	0.92768	5	2.39123	5	16.6165	36	191.841
			6	0.92767	6	2.39125	6	16.6168	37	191.839
			7	0.92767	7	2.39125	7	16.6168	38	191.839
0.5	∞	10	5	0.89872	5	2.22083	5	15.3669	27	187.825
			6	0.89509	6	2.22108	6	15.3676	28	187.828
			7	0.89509	7	2.22108	7	15.3676	29	187.828
0.2	0	30	5	1.51767	5	20.2430	5	634.589	5	11164.0
			6	1.52201	6	20.2484	6	634.439	6	11143.8
			7	1.52201	7	20.2484	7	634.439	7	11143.8
0.2	1	30	5	1.38205	5	10.5579	5	180.305	5	2830.08
			6	1.38201	6	10.5609	6	180.338	6	2830.32
			7	1.38201	7	10.5609	7	180.338	7	2830.32
0.2	∞	30	5	1.37101	7	10.0428	5	173.948	5	2809.22
			6	1.37103	8	10.0429	6	173.913	6	2807.15
			7	1.37103	9	10.0429	7	173.913	7	2807.15

Some collocation solutions for the dimensionless drag force $-F/6\pi\eta bU$ are presented in Table 3 for the translation of a prolate spheroid along its axis of revolution perpendicular to two equally distant plane walls [with $c/(c+d) = 1/2$] for various values of a/b , a/c , and $\eta/\beta b$. Analogous to Table 2 for the situation of the corresponding motion of a spheroid normal to a single plane wall, Table 3 indicates

that the boundary-corrected hydrodynamic drag force (or viscous retardation) on the spheroid increases monotonically with an increase in a/c for fixed values of a/b and $\eta/\beta b$ and with a decrease in $\eta/\beta b$ for given values of a/b and a/c . This outcome is also true for a general case with any given value of $c/(c+d)$ other than 0 and 1/2, whose results are not presented here but can also be obtained accurately.

Table 5: The dimensionless drag force experienced by an oblate spheroid situated midway between two parallel plane walls [$c/(c+d) = 1/2$] undergoing axisymmetric translation normal to the walls for various values of a/b , a/c , and $\eta/\beta b$

a/b	$\frac{\eta}{\beta b}$	M	$-F/6\pi\eta bU$							
			N	$a/c = 0.1$	N	$a/c = 0.5$	N	$a/c = 0.9$	N	$a/c = 0.99$
0.8	0	6	2	1.16102	2	3.35932	4	30.6078	68	374.98
			3	1.16102	3	3.35932	5	30.6079	69	374.76
			4	1.16102	4	3.35932	6	30.6079	70	374.76
0.8	1	6	2	0.86877	2	1.91081	3	10.6635	65	100.0
			3	0.86877	3	1.91082	4	10.6636	66	100.1
			4	0.86877	4	1.91082	5	10.6636	67	100.1
0.8	∞	6	2	0.79512	2	1.65240	3	9.35769	66	96.45
			3	0.79512	3	1.65241	4	9.35770	67	96.49
			4	0.79512	4	1.65241	5	9.35770	68	96.49
0.5	0	10	2	1.21662	2	6.02240	2	97.1386	17	1471.3
			3	1.21662	3	6.02247	3	97.1321	18	1465.6
			4	1.21662	4	6.02247	4	97.1321	19	1465.6
0.5	1	10	2	0.98478	2	3.44374	3	31.2923	30	381.57
			3	0.98478	3	3.44374	4	31.2924	31	381.58
			4	0.98478	4	3.44374	5	31.2924	32	381.58
0.5	∞	10	2	0.94820	2	3.15632	3	28.8703	35	373.635
			3	0.94821	3	3.15658	4	28.8705	36	373.636
			4	0.94821	4	3.15658	5	28.8705	37	373.636
0.2	0	30	3	1.74625	4	37.9093	4	1333.24	4	22263.9
			4	1.85259	5	37.9087	5	1264.42	5	22282.7
			5	1.85259	6	37.9087	6	1264.42	6	22282.7
0.2	1	30	4	1.65597	4	18.8196	4	356.277	5	5655.88
			5	1.65598	5	18.8198	5	356.486	6	5655.89
			6	1.65598	6	18.8198	6	356.486	7	5655.89
0.2	∞	30	4	1.64040	4	17.7996	4	345.743	4	5607.62
			5	1.64041	5	17.8000	5	343.649	5	5609.55
			6	1.64041	6	17.8000	6	343.649	6	5609.55

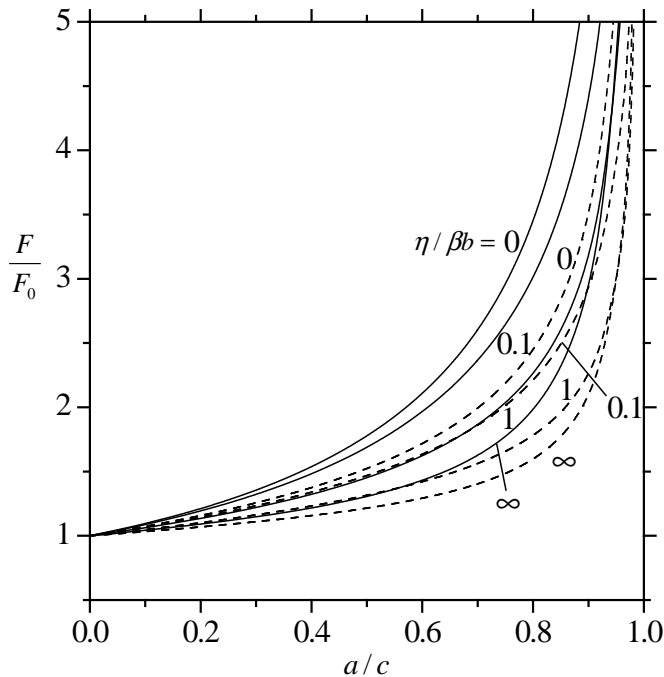


Figure 2: Plots of the normalized drag force F/F_0 for the translation of a prolate spheroid with $a/b = 2$ along its axis of revolution perpendicular to a single plane wall [$c/(c+d) \rightarrow 0$, dashed curves] and to two equally distant plane walls [$c/(c+d) = 1/2$, solid curves] versus the separation parameter a/c for various slip parameter $\eta/\beta b$.

The hydrodynamic drag force F exerted on a prolate spheroid with aspect ratio $a/b = 2$ translating along its axis of revolution perpendicular to a single plane wall [with $c/(c+d) = 0$] and to two equally distant plane walls [with $c/(c+d) = 1/2$] normalized by the corresponding drag force F_0 acting on the prolate spheroid when the walls are not present (as $a/c \rightarrow \infty$) as functions of the spacing parameter a/c for various values of $\eta/\beta b$ is plotted in Fig. 2. For a spheroid with given values of a/b (cases other than $a/b = 2$ are not displayed here for conciseness) and $\eta/\beta b$, the value of F/F_0 increases monotonically with an increase in the ratio a/c from $F/F_0 = 1$ at $a/c = 0$ to $F/F_0 \rightarrow \infty$ as $a/c \rightarrow 1$. In general, the normalized wall-corrected drag force on the spheroid decreases with an increase in $\eta/\beta b$, keeping a/b and a/c unchanged. It can be seen that the drag force on the spheroid can be large when a/c is close to unity and $\eta/\beta b$ is small.

Figures 3a and 3b show the collocation results for the normalized hydrodynamic

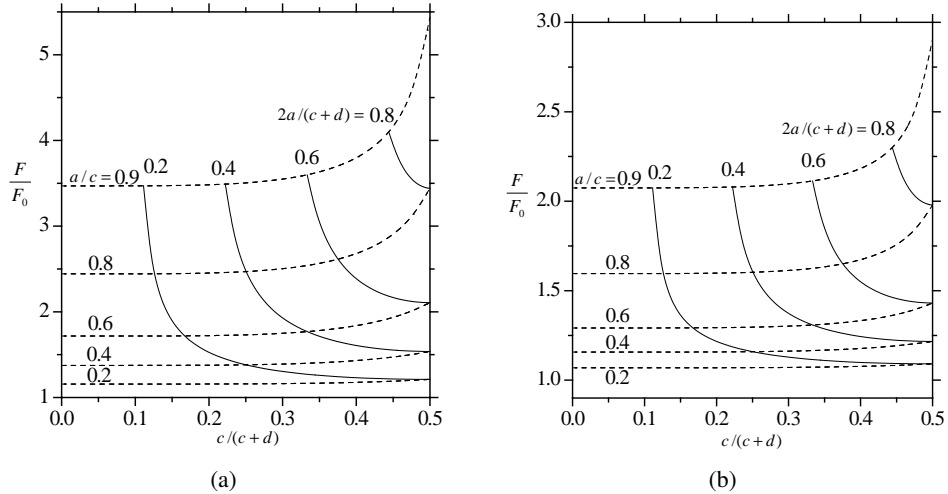


Figure 3: Plots of the normalized drag force F/F_0 for the translation of a prolate spheroid with $a/b = 2$ along its axis of revolution perpendicular to two plane walls versus the ratio $c/(c+d)$ with a/c and $2a/(c+d)$ as parameters: (a) no-slip spheroid ($\eta/\beta b = 0$); (b) perfect-slip spheroid ($\eta/\beta b \rightarrow \infty$).

drag force F/F_0 exerted on a prolate spheroid ($a/b = 2$) with no-slip condition ($\eta/\beta b = 0$) and perfect-slip condition ($\eta/\beta b \rightarrow \infty$), respectively, on its surface translating perpendicular to two plane walls at various positions between them. The dashed curves (with $a/c = \text{constant}$) illustrate the effect of the position of the second wall (at $z = d$, where $d \geq c$) on the drag force for various values of the relative sphere-to-wall spacing c/a . Evidently, the approach of a second wall will enhance the hydrodynamic drag experienced by the spheroid in the vicinity of the first wall. In general, for an arbitrary combination of parameters a/c and $\eta/\beta b$, the assumption that the results for two walls can be obtained by simple addition of the single-wall effects overestimates the correction to the hydrodynamic drag on a spheroid. The solid curves [with $2a/(c+d) = \text{constant}$] indicate the variation of the drag as a function of the particle position at various values of the relative wall-to-wall spacing $(c+d)/2a$. At a constant value of $2a/(c+d)$, analogous to the corresponding case of a spherical particle [Chang and Keh (2006)], the no-slip or perfect-slip spheroid (or a spheroid with a finite value of $\eta/\beta b$, whose result is not exhibited here) experiences a minimum drag when it is located midway between the two plane walls (with $d = c$), and the drag force increases monotonically as the particle approaches either of the walls.

The normalized drag force F/F_0 for the translation of a prolate spheroid situated

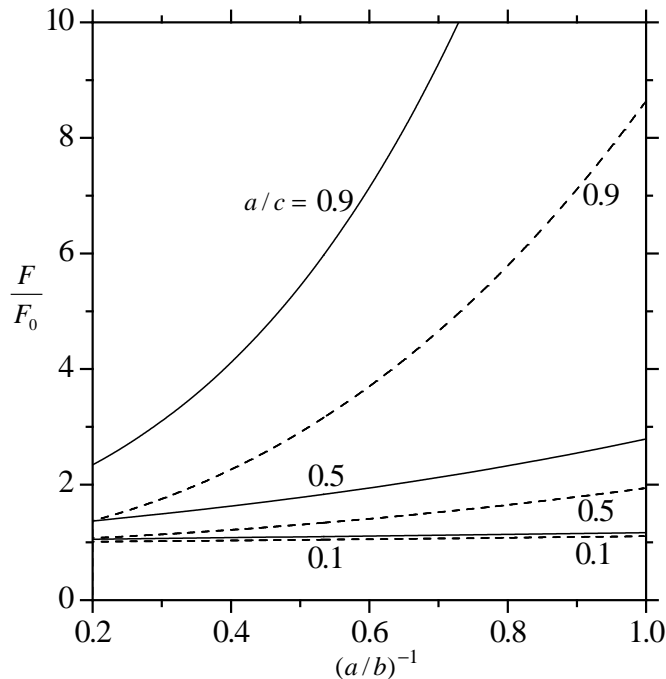


Figure 4: Plots of the normalized drag force F/F_0 for the translation of a prolate spheroid situated midway between two parallel plane walls ($d = c$) perpendicular to the walls versus the inverse aspect ratio $(a/b)^{-1}$ for different values of the separation parameter a/c . The solid and dashed curves represent the cases with no slip ($\eta/\beta b = 0$) and perfect slip ($\eta/\beta b \rightarrow \infty$), respectively.

midway between two parallel plane walls [with $c/(c+d) = 1/2$] perpendicular to the walls as a function of its aspect ratio a/b for various values of the spacing parameter a/c is plotted in Fig. 4. The solid and dashed curves represent the cases of translation of a no-slip spheroid (with $\eta/\beta b = 0$) and of a perfect-slip spheroid (with $\eta/\beta b \rightarrow \infty$), respectively. It can be seen that, due to the decrease of the effective particle-boundary interaction area that offers hydrodynamic resistance to the motion of the spheroid, F/F_0 decreases monotonically with an increase in a/b for given values of a/c and $\eta/\beta b$. For fixed values of a/b and a/c , as expected, a no-slip spheroid experiences more hydrodynamic drag than a slip spheroid does. Again, F/F_0 is a monotonically increasing function of a/c for specified values of a/b and $\eta/\beta b$.

6 Axisymmetric motion of an oblate particle normal to two plane walls

The translational motion of a slip axisymmetric prolate particle along its axis of revolution perpendicular to two infinite plane walls was considered in Section 4 and a set of spherical singularities must be distributed on a segment along the axis of revolution within the particle. In this section we consider the corresponding motion of a slip oblate particle and the spherical singularities should be distributed on the fundamental plane inside the particle. Since the oblate particle and the fluid motion are axisymmetric, the fundamental plane should be a circular disk S_d normal to the z -axis and with its center coinciding with the center of the particle (at the origin of the coordinate frame).

Let Q be an arbitrary point on S_d which is expressed with the cylindrical coordinates $\rho = \hat{\rho}$, $\phi = \hat{\phi}$, and $z = 0$. Then the velocity disturbance at another point $P(\rho = \rho^*, \phi = 0, z = z)$ generated by the spherical singularity at Q can be obtained using Eq. (4),

$$\hat{v}_\rho = \frac{\rho - \hat{\rho} \cos \hat{\phi}}{\rho^*} \sum_{n=2}^{\infty} [B_n A_{1n}(\rho^*, z, 0) + D_n A_{2n}(\rho^*, z, 0)], \quad (19a)$$

$$\hat{v}_\phi = \frac{\hat{\rho} \sin \hat{\phi}}{\rho^*} \sum_{n=2}^{\infty} [B_n A_{1n}(\rho^*, z, 0) + D_n A_{2n}(\rho^*, z, 0)], \quad (19b)$$

$$\hat{v}_z = \sum_{n=2}^{\infty} [B_n C_{1n}(\rho^*, z, 0) + D_n C_{2n}(\rho^*, z, 0)], \quad (19c)$$

where ρ^* is the distance from point Q to the projection of point P on the plane $z = 0$,

$$\rho^* = (\rho^2 + \hat{\rho}^2 - 2\rho\hat{\rho} \cos \hat{\phi})^{1/2}. \quad (20)$$

The total disturbance of the flow field produced by the oblate particle can be approximated by the superposition of the individual disturbances in Eq. (19) induced by the whole set of singularities on the fundamental disk S_d . Thus, at an arbitrary location in the fluid, we have the velocity components in integral form as

$$v_\rho = \sum_{n=2}^{\infty} \int_0^{2\pi} \int_0^R \frac{\rho - \hat{\rho} \cos \hat{\phi}}{\rho^*} [B_n(\hat{\rho}) A_{1n}(\rho^*, z, 0) + D_n(\hat{\rho}) A_{2n}(\rho^*, z, 0)] \hat{\rho} d\hat{\rho} d\hat{\phi}, \quad (21a)$$

$$v_z = \sum_{n=2}^{\infty} \int_0^{2\pi} \int_0^R [B_n(\hat{\rho}) C_{1n}(\rho^*, z, 0) + D_n(\hat{\rho}) C_{2n}(\rho^*, z, 0)] \hat{\rho} d\hat{\rho} d\hat{\phi}, \quad (21b)$$

where $v_\phi = 0$ and the unknown density distribution coefficients B_n and D_n are taken to be functions of $\hat{\rho}$ only due to the axial symmetry of the fluid motion, and R is the radius of the disk S_d . Eq. (21) provides an exact solution for Eq. (2) that satisfies Eqs. (3b) and (3c), and the unknown density distribution functions $B_n(\hat{\rho})$ and $D_n(\hat{\rho})$ must be determined from the remaining boundary condition (3a) or (5) using the multipole collocation method. In Eq. (5), the stress components can be calculated from Eq. (21) and expressed as

$$\begin{aligned} \tau_{\rho\rho} &= \eta \sum_{n=2}^{\infty} \int_0^{2\pi} \int_0^R \left\{ \frac{2\hat{\rho}^2 \sin^2 \hat{\phi}}{(\rho^*)^3} [B_n(\hat{\rho})A_{1n}(\rho^*, z, 0) + D_n(\hat{\rho})A_{2n}(\rho^*, z, 0)] \right. \\ &\quad \left. + \left(\frac{\rho - \hat{\rho} \cos \hat{\phi}}{\rho^*} \right)^2 [B_n(\hat{\rho})\alpha_{1n}(\rho^*, z, 0) + D_n(\hat{\rho})\alpha_{2n}(\rho^*, z, 0)] \right\} \hat{\rho} d\hat{\rho} d\hat{\phi}, \end{aligned} \quad (22a)$$

$$\tau_{zz} = \eta \sum_{n=2}^{\infty} \int_0^{2\pi} \int_0^R [B_n(\hat{\rho})\beta_{1n}(\rho^*, z, 0) + D_n(\hat{\rho})\beta_{2n}(\rho^*, z, 0)] \hat{\rho} d\hat{\rho} d\hat{\phi}, \quad (22b)$$

$$\tau_{\rho z} = \eta \sum_{n=2}^{\infty} \int_0^{2\pi} \int_0^R \frac{\rho - \hat{\rho} \cos \hat{\phi}}{\rho^*} [B_n(\hat{\rho})\gamma_{1n}(\rho^*, z, 0) + D_n(\hat{\rho})\gamma_{2n}(\rho^*, z, 0)] \hat{\rho} d\hat{\rho} d\hat{\phi}. \quad (22c)$$

From Eqs. (9) and (21), the drag force exerted by the fluid on the oblate particle is obtained by

$$F = 8\pi^2 \eta \int_0^R D_2(\hat{\rho}) \hat{\rho} d\hat{\rho}. \quad (23)$$

Similar to the case of the motion of a prolate particle examined in Section 4, the integrations in Eqs. (21) and (22) with respect to $\hat{\rho}$ can be approximated by the M -point Gauss-Legendre quadrature formula, as shown in Eq. (12), and each infinite series is truncated after N terms. Therefore, Eqs. (21) and (22) become

$$\begin{bmatrix} v_\rho \\ v_z \end{bmatrix} = \sum_{n=2}^{N+1} \sum_{m=1}^M \left\{ B_{nm} \begin{bmatrix} A_{1nm}(\rho, z, 0) \\ C_{1nm}(\rho, z, 0) \end{bmatrix} + D_{nm} \begin{bmatrix} A_{2nm}(\rho, z, 0) \\ C_{2nm}(\rho, z, 0) \end{bmatrix} \right\}, \quad (24a)$$

$$\begin{bmatrix} \tau_{\rho\rho} \\ \tau_{zz} \\ \tau_{\rho z} \end{bmatrix} = \eta \sum_{n=2}^{N+1} \sum_{m=1}^M \left\{ B_{nm} \begin{bmatrix} \alpha_{1nm}(\rho, z, 0) \\ \beta_{1nm}(\rho, z, 0) \\ \gamma_{1nm}(\rho, z, 0) \end{bmatrix} + D_{nm} \begin{bmatrix} \alpha_{2nm}(\rho, z, 0) \\ \beta_{2nm}(\rho, z, 0) \\ \gamma_{2nm}(\rho, z, 0) \end{bmatrix} \right\}, \quad (24b)$$

where the functions A_{inm} , C_{inm} , α_{inm} , β_{inm} , and γ_{inm} with $i = 1$ and 2 are defined by Eqs. (A18) and (A19), and B_{nm} and D_{nm} are the unknown density constants.

Application of the boundary condition (5) to Eqs. (24) and (25) yields

$$\sum_{n=2}^{N+1} \sum_{m=1}^M \{B_{nm} \begin{bmatrix} A_{1nm}^*(\rho, z, 0) \\ C_{1nm}^*(\rho, z, 0) \end{bmatrix} + D_{nm} \begin{bmatrix} A_{2nm}^*(\rho, z, 0) \\ C_{2nm}^*(\rho, z, 0) \end{bmatrix}\} = \begin{bmatrix} 0 \\ U \end{bmatrix} \text{ on } S_p, \quad (25)$$

where A_{inm}^* and C_{inm}^* with $i = 1$ and 2 are given by Eq. (8) with the subscript n of its functions being replaced by nm . Thus, the collocation technique described in Section 4 can be used to satisfy the boundary condition (26) and to determine the $2MN$ density constants B_{nm} and D_{nm} required for the fluid velocity field. Once these constants are determined, the drag force acting on the particle by the fluid can be obtained from Eq. (23), with the result

$$F = 8\pi^2 \eta \sum_{m=1}^M D_{2m}. \quad (26)$$

7 Solution for the axisymmetric motion of an oblate spheroid normal to two plane walls

The numerical solutions of the hydrodynamic drag force experienced by a prolate spheroid translating along its axis of revolution perpendicular to one or two plane walls were presented in Section 5. In this section the similar singularity method and collocation technique described in the previous section will be used to solve the corresponding motion of an oblate spheroid. The surface of the oblate spheroid and the local components of its unit normal vector \mathbf{n} can still be represented by Eqs. (17) and (18), but now with $0 < a/b < 1$. The numerical results of the nondimensional hydrodynamic drag force $-F/6\pi\eta bU$ for the translation of an oblate spheroid along its axis of revolution perpendicular to a single plane wall [with $c/(c+d) = 0$] and to two equally distant plane walls [with $c/(c+d) = 1/2$] are presented in Tables 4 and 5, respectively, for various values of the aspect ratio a/b , spacing parameter a/c , and slip parameter $\eta/\beta b$. The values of $-F/6\pi\eta bU$ are computed for different values of N and M in Eqs. (24)-(27) (which shows convergence tests). To achieve good convergence behavior for the calculation of F , the larger value of N is in general required when the particle is located closer to the plane wall, whereas the larger value of M is needed when the axial-to-radial aspect ratio a/b of the oblate spheroid becomes smaller. For the special case of a no-slip spheroid (with $\eta/\beta b = 0$) translating along its axis of revolution normal to a single plane wall, the agreement between our results and the previous numerical solutions obtained by Hsu and Ganatos (1989) and Keh and Tseng (1994) is excellent. Analogous to Tables 2 and 3 for the corresponding motion of a prolate spheroid perpendicular to two plane walls, Tables 4 and 5 indicate that $-F/6\pi\eta bU$ increases

monotonically with an increase in a/c for specific values of a/b , $c/(c+d)$, and $\eta/\beta b$ and with a decrease in $\eta/\beta b$ for constant values of a/b , $c/(c+d)$, and a/c . The hydrodynamic drag force F experienced by an oblate spheroid with aspect ratio $a/b = 1/2$ translating along its axis of revolution perpendicular to a single plane wall and to two equally distant plane walls normalized by the corresponding drag force F_0 acting on an unbounded oblate spheroid (with $a/c \rightarrow \infty$) as functions of a/c for various values of $\eta/\beta b$ is plotted in Fig. 5. Analogous to the case of a prolate spheroid discussed in Section 5, for an oblate spheroid with given aspect ratio (cases other than $a/b = 1/2$ are not illustrated here for conciseness), the value of F/F_0 increases monotonically with an increase in a/c and in general decreases with an increase in $\eta/\beta b$, keeping the other parameters unchanged. It can be seen that the drag force exerted on the oblate spheroid can be very large when a/c is close to unity, especially as the value of $\eta/\beta b$ is small. Again, $F/F_0 = 1$ as $a/c = 0$ and $F/F_0 \rightarrow \infty$ as $a/c \rightarrow 1$.

The collocation results for the normalized hydrodynamic drag force F/F_0 acting on an oblate spheroid ($a/b = 1/2$) with no-slip condition ($\eta/\beta b = 0$) and perfect-slip condition ($\eta/\beta b \rightarrow \infty$) on its surface moving perpendicular to two plane walls at various positions between them are plotted in Fig. 6. Again, at a constant value of $2a/(c+d)$, the no-slip or perfect-slip particle (or a particle with a finite value of $\eta/\beta b$, whose results are not displayed here) experiences a minimum drag when it is located midway between the two plane walls (with $d = c$), and the drag force increases monotonically as the particle approaches either of the walls.

In Fig. 7, the normalized drag force F/F_0 for the axisymmetric translation of an oblate spheroid situated midway between two parallel plane walls (with $d = c$) as a function of the aspect ratio a/b for different values of the spacing parameter a/c is plotted. The solid and dashed curves denote the cases of translation of a no-slip spheroid (with $\eta/\beta b = 0$) and of a perfect-slip spheroid (with $\eta/\beta b \rightarrow \infty$), respectively. Similarly to the boundary effects on the motion of a prolate spheroid, F/F_0 for a confined oblate spheroid increases monotonically as the ratio a/b decreases or a/c increases, keeping other factors fixed. Again, a no-slip spheroid experiences more hydrodynamic drag than a slip spheroid does for specified values of a/b and a/c .

8 Concluding remarks

In this article, the creeping motion caused by the translation of a general axisymmetric particle with a slip surface in a viscous fluid along its axis of revolution perpendicular to one or two plane walls has been examined by the use of the method of internal singularity distributions combined with the boundary collocation tech-

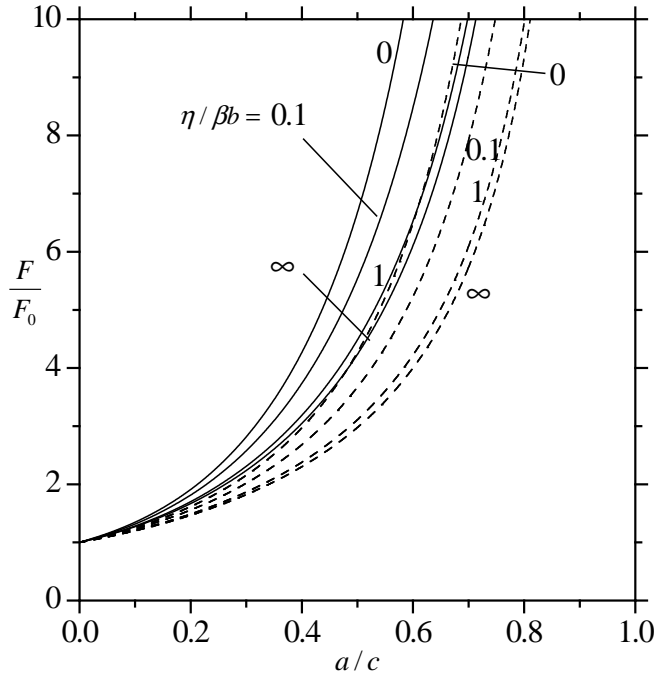


Figure 5: Plots of the normalized drag force F/F_0 for the translation of an oblate spheroid with $a/b = 1/2$ along its axis of revolution perpendicular to a single plane wall [$c/(c+d) \rightarrow 0$, dashed curves] and to two equally distant plane walls [$c/(c+d) = 1/2$, solid curves] versus the separation parameter a/c for various slip parameter $\eta/\beta b$.

nique. For the case of the axisymmetric motion of a prolate particle, a truncated set of spherical singularities is distributed along the axis within the particle, whereas for the case of an oblate particle, the spherical singularities are placed on the fundamental disk of the particle. The numerical results for the drag force acting on the particle by the fluid indicate that the solution procedure converges rapidly and accurate solutions can be obtained for various cases of the particle shape, slippage, and separation from the walls. Although the numerical solutions were presented in the previous sections only for the translation of a sphere, a prolate spheroid, and an oblate spheroid, the combined analytical and numerical method utilized in this work can easily provide the hydrodynamic calculations for the motion of an axially symmetric particle of other shapes, such as a prolate or oblate Cassini oval [Keh and Tseng (1994)].

In Tables 1-5 and Figs. 2-7, we presented only the results for the resistance prob-

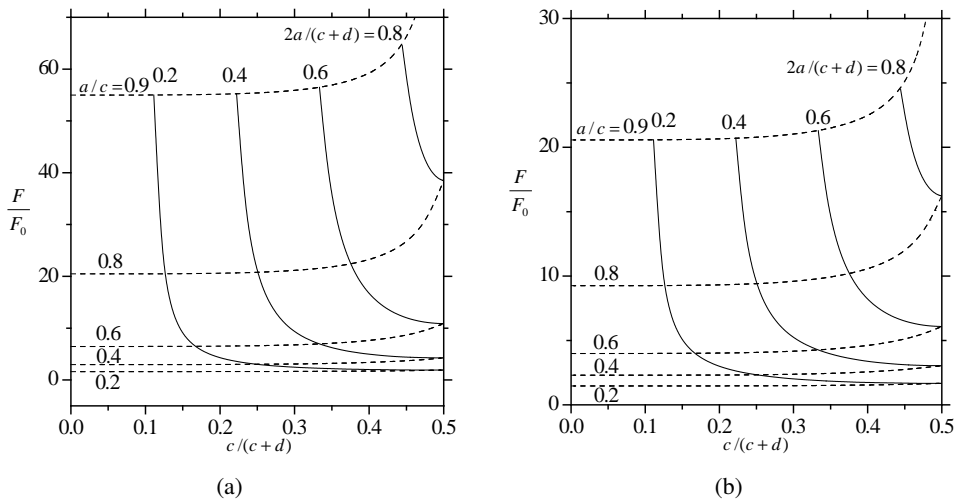


Figure 6: Plots of the normalized drag force F/F_0 for the translation of an oblate spheroid with $a/b = 1/2$ along its axis of revolution perpendicular to two plane walls versus the ratio $c/(c+d)$ with a/c and $2a/(c+d)$ as parameters: (a) no-slip spheroid ($\eta/\beta b = 0$); (b) perfect-slip spheroid ($\eta/\beta b \rightarrow \infty$).

lems, defined as those in which the drag force F exerted by the surrounding fluid on the translating particle is to be determined for a specified particle velocity U . In a mobility problem, on the other hand, the external force F imposed on the particle is specified and the particle velocity U is to be determined. It is worth to note that our results can also be used for those physical problems in which the applied force on the particle is the prescribed quantity and the particle must move accordingly.

Acknowledgement: Part of this research was supported by the National Science Council of the Republic of China.

Appendix A: Definitions of functions in Sections 2 and 6

For conciseness the definitions of some functions in Sections 2 and 6 are listed in this appendix. The functions appearing in Eqs. (4) and (6) in Section 2 are defined

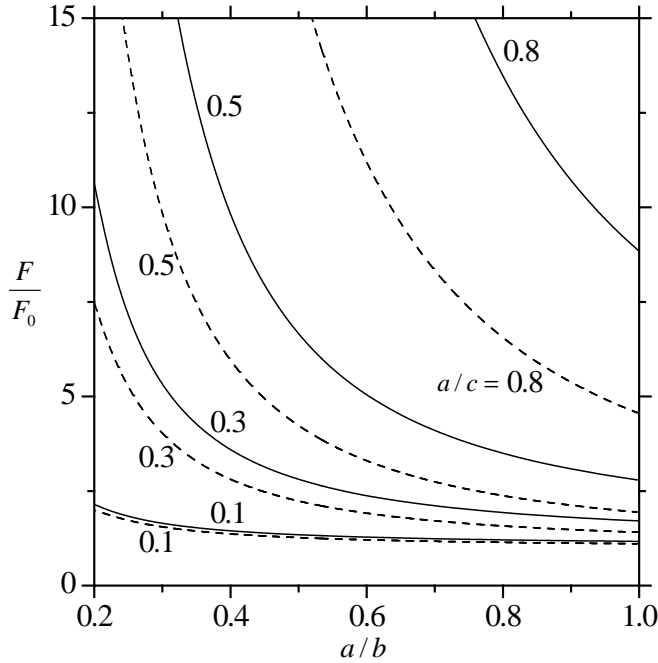


Figure 7: Plots of the normalized drag force F/F_0 for the translation of an oblate spheroid situated midway between two parallel plane walls ($d = c$) perpendicular to the walls versus the aspect ratio a/b for different values of the separation parameter a/c . The solid and dashed curves represent the cases with no slip ($\eta/\beta b = 0$) and perfect slip ($\eta/\beta b \rightarrow \infty$), respectively.

as

$$A_{in}(\rho, z, h) = - \int_0^\infty E_{in}(\omega, z, h) J_1(\omega \rho) d\omega - \rho^{-1} r_h^{-n+2i-2} [(n+1) G_{n+1}^{-1/2}(\xi) - 2(i-1) \xi G_n^{-1/2}(\xi)], \quad (\text{A1})$$

$$C_{in}(\rho, z, h) = - \int_0^\infty F_{in}(\omega, z, h) J_0(\omega \rho) d\omega - r_h^{-n+2i-3} [P_n(\xi) + 2(i-1) G_n^{-1/2}(\xi)]; \quad (\text{A2})$$

$$\begin{aligned} \alpha_{in}(\rho, z, h) = & - \int_0^\infty E_{in}(\omega, z, h) [J_0(\omega\rho) - J_2(\omega\rho)] \omega d\omega \\ & - 2\rho^{-2} r_h^{-n+2i-4} \{ (n+1)[(-n+2i-2)\rho^2 - r_h^2] G_{n+1}^{-1/2}(\xi) + (n+1)\rho^2 \xi P_n(\xi) \\ & + 2(i-1)[r_h^2 + (n-2i+3)\rho^2] \xi G_n^{-1/2}(\xi) - 2(i-1)\rho^2 \xi^2 P_{n-1}(\xi) \}, \quad (\text{A3}) \end{aligned}$$

$$\begin{aligned} \beta_{in}(\rho, z, h) = & -2 \int_0^\infty H_{in}(\omega, z, h) J_0(\omega\rho) d\omega - 2r_h^{-n+2i-4} \{ (-2n+2i-3) \xi P_n(\xi) \\ & + nP_{n-1}(\xi) + 2(i-1)[(-n+2i-3)\xi G_n^{-1/2}(\xi) - (1-\xi^2)P_{n-1}(\xi)] \}, \quad (\text{A4}) \end{aligned}$$

$$\begin{aligned} \gamma_{in}(\rho, z, h) = & - \int_0^\infty [T_{in}(\omega, z, h) - F_{in}(\omega, z, h)\omega] J_1(\omega\rho) d\omega \\ & - \rho^{-1} r_h^{-n+2i-5} \{ (n+1)(-n+2i-2)r_h^2 \xi G_{n+1}^{-1/2}(\xi) + [2(-n+i-2)\rho^2 + nz_h^2] P_n(\xi) \\ & - nr_h^2 \xi P_{n-1}(\xi) + 2(i-1)[\{(-n+2i-3)(\rho^2 - z_h^2) - r_h^2\} G_n^{-1/2}(\xi) + 2\rho^2 \xi P_{n-1}(\xi)] \}, \quad (\text{A5}) \end{aligned}$$

where i equals 1 or 2,

$$\begin{aligned} \begin{bmatrix} E_{in}(\omega, z, h) \\ F_{in}(\omega, z, h) \\ T_{in}(\omega, z, h) \\ H_{in}(\omega, z, h) \end{bmatrix} = & \omega \left\{ \begin{bmatrix} G''_+(\sigma, \eta) \\ -G'_-(\sigma, \eta) \\ G^{**}_+(\sigma, \eta) \\ -G^*_-(\sigma, \eta) \end{bmatrix} B'_{in}(\omega, -c-h) + \begin{bmatrix} -G''_+(\eta, \sigma) \\ G'_-(\eta, \sigma) \\ -G^{**}_+(\eta, \sigma) \\ G^*_-(\eta, \sigma) \end{bmatrix} B'_{in}(\omega, d-h) \right. \\ & \left. + \begin{bmatrix} -G'_+(\sigma, \eta) \\ G''_-(\sigma, \eta) \\ -G^*_+(\sigma, \eta) \\ G^{**}_-(\sigma, \eta) \end{bmatrix} B''_{in}(\omega, -c-h) + \begin{bmatrix} G'_+(\eta, \sigma) \\ -G''_-(\eta, \sigma) \\ G^*_+(\eta, \sigma) \\ -G^{**}_-(\eta, \sigma) \end{bmatrix} B''_{in}(\omega, d-h) \right\}; \quad (\text{A6}) \end{aligned}$$

$$B'_{1n}(\omega, z) = -\frac{1}{n!} \left(\frac{\omega |z|}{z} \right)^{n-1} e^{-\omega|z|}, \quad (\text{A7})$$

$$B''_{1n}(\omega, z) = -\frac{\omega^{n-1}}{n!} \left(\frac{|z|}{z} \right)^n e^{-\omega|z|}, \quad (\text{A8})$$

$$B'_{2n}(\omega, z) = -\frac{1}{n!} \left(\frac{\omega |z|}{z} \right)^{n-3} [(2n-3)\omega |z| - n(n-2)] e^{-\omega|z|}, \quad (\text{A9})$$

$$B''_{2n}(\omega, z) = -\frac{\omega^{n-3}}{n!} \left(\frac{|z|}{z} \right)^n [(2n-3)\omega |z| - (n-1)(n-3)] e^{-\omega|z|}; \quad (\text{A10})$$

$$G'_{\pm}(\mu, v) = \tau^* \mu v (\mu' \pm \tau' v'), \quad (\text{A11})$$

$$G''_{\pm}(\mu, v) = \tau^* [v(\cosh \mu - \tau' v') \pm \mu(\mu' - \tau' \cosh v)], \quad (\text{A12})$$

$$G^*_{\pm}(\mu, v) = \tau^* \omega [\sinh \mu + v \cosh \mu \pm \tau' (\sinh v + \mu \cosh v)], \quad (\text{A13})$$

$$G^{**}_{\pm}(\mu, v) = \tau^* \omega \{ \cosh \mu + v \sinh \mu - \tau' \cosh v \pm [\cosh \mu - \tau' (\cosh v + \mu \sinh v)] \}; \quad (\text{A14})$$

$$\mu' = \frac{\sinh \mu}{\mu}, \quad v' = \frac{\sinh v}{v}, \quad \tau' = \frac{\sinh \tau}{\tau}, \quad \tau^* = \frac{\tau}{\sinh^2 \tau - \tau^2}, \quad (\text{A15})$$

$$\sigma = \omega(z+c), \quad \eta = \omega(z-d), \quad \tau = \omega(c+d), \quad (\text{A16})$$

$$r_h = (\rho^2 + z_h^2)^{1/2}, \quad z_h = z - h, \quad \xi = z_h/r_h, \quad (\text{A17})$$

J_n is the Bessel function of the first kind of order n , $G_n^{-1/2}$ is the Gegenbauer polynomial of the first kind of order n and degree $-1/2$, and P_n is the Legendre polynomial of order n .

The following are the definitions of some functions used in Eqs. (24) and (25) in Section 6:

$$\begin{bmatrix} A_{inm}(\rho, z, h) \\ C_{inm}(\rho, z, h) \end{bmatrix} = \int_0^{2\pi} \begin{bmatrix} \frac{\rho - q_m \cos \hat{\phi}}{\rho_m^*} A_{in}(\rho_m^*, z, h) \\ C_{in}(\rho_m^*, z, h) \end{bmatrix} d\hat{\phi}, \quad (\text{A18})$$

$$\begin{bmatrix} \alpha_{inm}(\rho, z, h) \\ \beta_{inm}(\rho, z, h) \\ \gamma_{inm}(\rho, z, h) \end{bmatrix} = \int_0^{2\pi} \begin{bmatrix} \frac{2q_m^2 \sin^2 \hat{\phi}}{(\rho_m^*)^3} A_{in}(\rho_m^*, z, h) + (\frac{\rho - q_m \cos \hat{\phi}}{\rho_m^*})^2 \alpha_{in}(\rho_m^*, z, h) \\ \beta_{in}(\rho_m^*, z, h) \\ \frac{\rho - q_m \cos \hat{\phi}}{\rho_m^*} \gamma_{in}(\rho_m^*, z, h) \end{bmatrix} d\hat{\phi}, \quad (\text{A19})$$

where $\rho_m^* = (\rho^2 + q_m^2 - 2q_m \rho \cos \hat{\phi})^{1/2}$, and q_m are the quadrature zeros referred to Eq. (12). The integrations in Eqs. (A18) and (A19) can be performed numerically after the substitution of Eqs. (A1)-(A5).

References

- Basset, A. B.** (1961): *A treatise on hydrodynamics, volume 2*. Dover, New York.
- Brenner, H.** (1966): The Stokes resistance of an arbitrary particle – Part V. Symbolic operator representation of intrinsic resistance. *Chem. Eng. Sci.*, 21, 97-109.
- Chang, Y. C.; Keh, H. J.** (2006): Slow motion of a slip spherical particle perpendicular to two plane walls. *J. Fluids Structures*, 22, 647-661.

- Chang, Y. C.; Keh, H. J.** (2009): Translation and rotation of slightly deformed colloidal spheres experiencing slip. *J. Colloid Interface Sci.*, 330, 201-210.
- Chen, P. Y.; Keh, H. J.** (2003): Slow motion of a slip spherical particle parallel to one or two plane walls. *J. Chin. Inst. Chem. Engrs.*, 34, 123-133.
- Chwang, A. T.; Wu, T. Y.** (1975): Hydrodynamic of low-Reynolds-number flow, Part 2. Singularity method for Stokes flows. *J. Fluid Mech.*, 67, 787-815.
- Dahneke, B. E.** (1973): Slip correction factors for nonspherical bodies-III. The form of the general law. *J. Aerosol Sci.* 4, 163-170.
- Deo, S.; Datta, S.** (2002): Slip flow past a prolate spheroid. *Indian J. Pure Appl. Math.* 33, 903-909.
- Ganatos, P.; Weinbaum, S.; Pfeffer, R.** (1980): A strong interaction theory for the creeping motion of a sphere between plane parallel boundaries. Part 1. Perpendicular motion. *J. Fluid Mech.* 99, 739-753.
- Gluckman, M. J.; Pfeffer, R.; Weinbaum, S.** (1971): A new technique for treating multi-particle slow viscous flow: axisymmetric flow past spheres and spheroids. *J. Fluid Mech.*, 50, 705-740.
- Happel, J.; Brenner, H.** (1983): *Low Reynolds number hydrodynamics*. Nijhoff, The Netherlands.
- Hornbeck, R. W.** (1975): *Numerical Methods*. Quantum Publishers, New York.
- Hsu, R.; Ganatos, P.** (1989): The motion of a rigid body in viscous fluid bounded by a plane wall. *J. Fluid Mech.*, 207, 29-72.
- Hu, C. M.; Zwanzig, R.** (1974): Rotational friction coefficients for spheroids with the slipping boundary condition. *J. Chem. Phys.*, 60, 4354-4357.
- Hutchins, D. K.; Harper, M. H.; Felder, R. L.** (1995): Slip correction measurements for solid spherical particles by modulated dynamic light scattering. *Aerosol Sci. Technol.*, 22, 202-218.
- Keh, H. J.; Chang, Y. C.** (2007): Slow motion of a slip spherical particle in a circular cylindrical pore. *Int. J. Multiphase Flow*, 33, 726-741.
- Keh, H. J.; Chang, Y. C.** (2008): Slow motion of a slip spheroid along its axis of revolution. *Int. J. Multiphase Flow*, 34, 713-722.
- Keh, H. J.; Huang, C. H.** (2004): Slow motion of axisymmetric slip particles along their axes of revolution. *Int. J. Eng. Sci.*, 42, 1621-1644.
- Keh, H. J.; Tseng, C. H.** (1994): Slow motion of an arbitrary axisymmetric body along its axis of revolution and normal to a plane surface. *Int. J. Multiphase Flow*, 20, 185-210.
- Keh, H. J.; Wang, L. J.** (2008): Slow motion of a circular cylinder experiencing

- slip near a plane wall. *J. Fluids Structures*, 24, 651-663.
- Leong, K. H.** (1984): Thermophoresis and diffusiophoresis of large aerosol particles of different shapes. *J. Aerosol Sci.*, 15, 511-517.
- Nir, A.** (1976): Linear shear flow past a porous particle. *Appl. Sci. Res.*, 32, 313-325.
- Oberbeck, A.** (1876): Über stationare Flüssigkeitsbewegungen mit Berücksichtigung der inneren Reibung. *J. Reine Angew. Math.*, 81, 62-80.
- O'Brien, V.** (1968): Form factors for deformed spheroids in Stokes flow. *AICHE Journal*, 14, 870-875.
- Palaniappan, D.** (1994): Creeping flow about a slightly deformed sphere. *ZAMP*, 45, 832-838.
- Ramkisson, H.** (1997): Slip flow past an approximate spheroid. *Acta Mech.*, 123, 227-233.
- Saffman, P. G.** (1971): On the boundary condition at the surface of a porous medium. *Studies Appl. Math.*, 50, 93-101.
- Sellier, A.** (2008): Slow viscous motion of a solid particle in a spherical cavity. *CMES: Computer Modeling in Engineering & Sciences*, vol. 25, 165-179.
- Sherif, H. H.; Faltas, M. S.; Saad, E. I.** (2008): Slip at the surface of a sphere translating perpendicular to a plane wall in micropolar fluid. *Z. Angew. Math. Phys.*, 59, 293-312.
- Staben, M. E.; Zinchenko A. Z.; Davis, R. H.** (2003): Motion of a particle between two parallel plane walls in low-Reynolds-number Poiseuille flow. *Phys. Fluids*, 15, 1711-1733.
- Stokes, G. G.** (1851): On the effect of the internal friction of fluid on pendulums. *Trans. Cambridge Phil. Soc.*, 9, 8-106.
- Tretheway, D. C.; Meinhart, C. D.** (2002): Apparent fluid slip at hydrophobic microchannel walls. *Phys. Fluids*, 14, L9-L12.
- Wan, Y. W.; Keh, H. J.** (2010): Slow rotation of an axisymmetric slip particle about its axis of revolution. *CMES: Computer Modeling in Engineering & Sciences*, vol. 53, 73-93.
- Williams, M. M. R.** (1986): Thermophoretic forces acting on a spheroid. *J. Phys. D: Appl. Phys.*, 19, 1631-1642.
- Willmott, G.** (2008): Dynamics of a sphere with inhomogeneous slip boundary conditions in Stokes flow. *Phys. Rev. E*, 77, 055302-1-4.
- Ying, R.; Peters M. H.** (1991): Interparticle and particle-surface gas dynamic interactions. *Aerosol Sci. Technol.*, 14, 418-433.

